European Radiology (2023) 33:1949–1962
https://doi.org/10.1007/s00330-022-09153-z

ONCOLOGY

Development and validation of a deep learning signature for predicting lymph node metastasis in lung adenocarcinoma: comparison with radiomics signature and clinical-semantic model

Xiaoling Ma[1] · Liming Xia[2] · Jun Chen[3] · Weijia Wan[2] · Wen Zhou[2]

Received: 27 April 2022 / Revised: 23 July 2022 / Accepted: 8 September 2022 / Published online: 28 September 2022

Abstract

Objective To develop and validate a deep learning (DL) signature for predicting lymph node (LN) metastasis in patients with lung adenocarcinoma.

Methods A total of 612 patients with pathologically-confirmed lung adenocarcinoma were retrospectively enrolled and were randomly divided into training cohort (n = 489) and internal validation cohort (n = 123). Besides, 108 patients were enrolled and constituted an independent test cohort (n = 108). Patients' clinical characteristics and CT semantic features were collected. The radiomics features were derived from contrast-enhanced CT images. The clinical-semantic model and radiomics signature were built to predict LN metastasis. Furthermore, Swin Transformer was adopted to develop a DL signature predictive of LN metastasis. Model performance was evaluated by area under the receiver operating characteristic curve (AUC), sensitivity, specificity, calibration curve, and decision curve analysis. The comparisons of AUC were conducted by the DeLong test.

Results The proposed DL signature yielded an AUC of 0.948–0.961 across all three cohorts, significantly superior to both clinical-semantic model and radiomics signature (all $p < 0.05$). The calibration curves show that DL signature predicted probabilities fit well the actual observed probabilities of LN metastasis. DL signature gained a higher net benefit than both clinical-semantic model and radiomics signature. The incorporation of radiomics signature or clinical-semantic risk predictors failed to reveal an incremental value over the DL signature.

Conclusions The proposed DL signature based on Swin Transformer achieved a promising performance in predicting LN metastasis and could confer important information in noninvasive mediastinal LN staging and individualized therapeutic options.

Key Points

- *Accurate prediction for lymph node metastasis is crucial to formulate individualized therapeutic options for patients with lung adenocarcinoma.*
- *The deep learning signature yielded an AUC of 0.948–0.961 across all three cohorts in predicting lymph node metastasis, superior to both radiomics signature and clinical-semantic model.*
- *The incorporation of radiomics signature or clinical-semantic risk predictors into deep learning signature failed to reveal an incremental value over deep learning signature.*

Keywords Lung adenocarcinoma · Computer tomography · Deep learning · Radiomics · Lymph node

✉ Liming Xia
xialiming2017@outlook.com

[1] Medical Imaging Center, People's Hospital of Ningxia Hui Autonomous Region, Yinchuan, China

[2] Department of Radiology, Tongji Hospital, Tongji Medical College, Huazhong University of Science and Technology, 1095 Jiefang Road, Qiaokou District, Wuhan 430030, Hubei, China

[3] GE Healthcare, Wuhan, China

Abbreviations

AUC	Area under the curve
CEA	Carcinoembryonic antigen
CI	Confidence interval
CS	Clinical-semantic
CTR	Consolidation-to-tumor ratio
DL	Deep learning
ICC	Intraclass correlation coefficient
LI	Labeling index
LN	lymph node

NSCLC Non-small cell lung cancer
OR Odds ratio
ROC Receiver operating characteristic curve

Introduction

Lung cancer remains the leading cause of cancer-related death globally and imposes a huge burden on human health and economics [1]. Anatomic lobectomy and systematic lymph node (LN) dissection are the standard surgical procedure for resectable non-small cell lung cancer (NSCLC). Sublobectomy could preserve more lung tissue, reduce operation trauma, and improve postoperative living quality. Multiple studies demonstrated that sublobectomy could provide the therapeutic effect equivalent to lobectomy for early-stage NSCLC patients [2–4]. Accurate presurgical prediction of LN status is beneficial to choose segmentectomy or wedge resection for node-negative, early-stage patients. Especially, LN status assessment was impracticable during wedge resection, so no LN metastasis should be confirmed prior to operation [5, 6]. Additionally, for patients scheduled for radiotherapy, accurate mediastinal staging could assist oncologists in designating irradiation fields, reducing the risk of treatment failure due to occult LN metastasis. Thus, accurate prediction of LN metastasis is crucial in informing therapeutic decision-making for NSCLC patients.

The endobronchial ultrasound-guided transbronchial needle aspiration or mediastinoscopy are generally used to pathologically confirm LN metastasis. However, these invasive methods could not be routinely applied across the whole population due to complications such as airway bleeding, pneumothorax, or nerve injury [7]. Pretreatment LN staging is noninvasively evaluated through imaging modalities including CT and PET/CT, but CT interpretation of LN short-axis diameter has been proved to be implausible in diagnosing LN metastasis [8]; For PET/CT, LN false positives caused by inflammation and granuloma, as well as expensive fees, were obstacles to a wide clinical application of this modality [9, 10]. Recently, several scholars developed CT-based radiomics predictors for LN metastasis [11–14]. But the radiomics approach needs handcraft segmentation of tumors, which is labor-intensive and time-consuming. Furthermore, radiomics features are highly susceptible to the heterogeneity of interobserver segmentation due to subjective judgement and professional skill [15].

Encouragingly, the emerging deep learning (DL) has achieved inspiring marks in differentiating histological subtypes [16, 17], evaluating therapeutic response [18–20], and predicting outcomes for lung cancer [21, 22]. DL approach could automatically extract representative information without manual segmentation. A few scholars previously applied the DL approach to predict LN metastasis for NSCLC. However, their studies had relatively small sample sizes and some important clinical variables such as smoking history and carcinoembryonic antigen (CEA) status were not involved. Besides, their constructed DL models did not perform remarkably well and still need to be improved [23–25]. Lung adenocarcinoma is the most common histological subtype of lung cancer, accounting for nearly 60% of NSCLC [26]. This study adopted a novel DL architecture named Swin Transformer to develop and validate a DL signature predictive of mediastinal LN invasion in patients with lung adenocarcinoma. We also compared the predictive performance of DL with traditional radiomics signature and clinical-semantic (CS) model based on clinical characteristics and CT semantic features in risk estimation of LN metastasis.

Methods and materials

Patients

This retrospective study was approved by the institutional ethics committee and the requirement for informed consent was waived. The patients undergoing radical surgical excision and systematic lymphadenectomy from May 2014 to September 2019 were retrospectively reviewed. We included patients with (1) pathologically-confirmed primary lung adenocarcinoma; (2) no presurgical radiotherapy or chemotherapy; (3) the interval time from presurgical CT examination to operation within 2 weeks. The exclusion criteria were as follows: (a) adenocarcinoma in situ, minimally invasive adenocarcinoma, and rare histological variants of lung adenocarcinoma; (b) synchronous or metachronous tumors; (c) no thin-section CT image or unsatisfactory CT image quality; (d) incomplete clinicopathologic data; (e) histories of other cancers. Finally, 612 patients were enrolled and then randomly divided into training cohort (n = 489) and internal validation cohort (n = 123) at a ratio of 4:1. Following the same eligibility criteria, 108 eligible patients receiving surgical excision in our institution from October 2019 to January 2021 were collected to constitute an independent test cohort (n = 108). The patient recruitment was shown in Fig. 1.

The clinicopathological characteristics including age, gender, smoking history, pack-year and serum CEA status, histological subtypes, Ki-67 labeling index (LI), and LN status were acquired from electrical medical records. Histological grade is determined by the prognostic classification of the predominant histological subtype of lung adenocarcinoma [27, 28].

CT acquisition and semantic features interpretation

The patients underwent contrast-enhanced CT examination using two multi-slice spiral CT scanners (GE Discovery CT 750 HD, TOSHIBA Aquilion One TSX-301A). The CT acquisition parameters were revealed in Supplementary data.

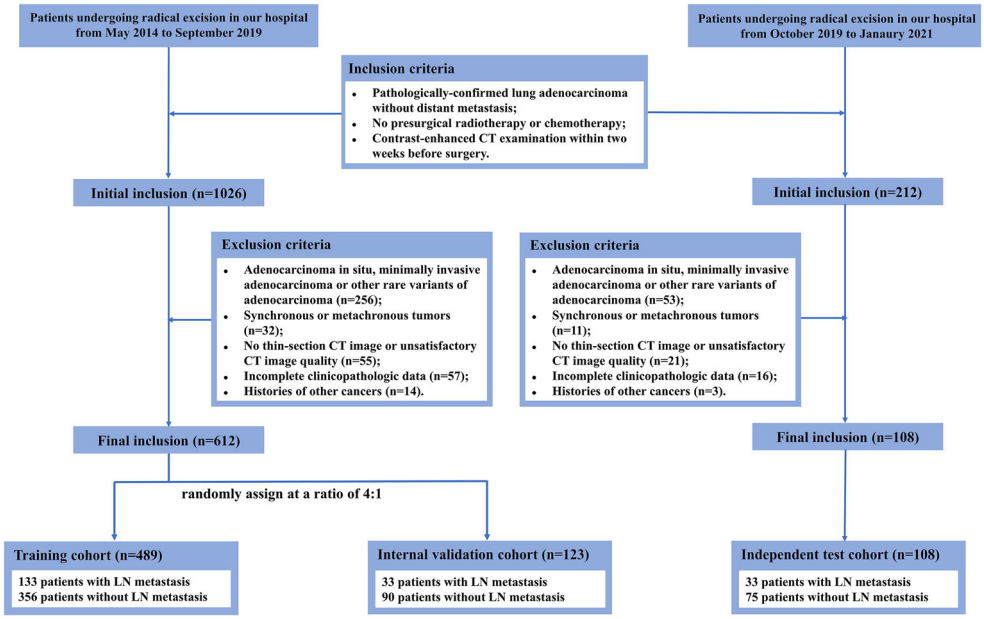

Fig. 1 The workflow diagram of patient recruitment

Blinded to clinicopathologic information, two radiologists with experience of 8 years and 3 years independently assessed CT semantic features in fixed lung window (width, 1600 HU; level, −600 HU) and mediastinal window (width, 400 HU; level, 40 HU). CT semantic features included location, affiliated lobe, tumor total diameter, tumor consolidation diameter, consolidation-to-tumor ratio (CTR), spiculation, lobulation, air bronchogram, plural attachment, and CT-reported LN status. CTR was calculated with the following formula: CTR (%) = tumor consolidation diameter /tumor total diameter × 100 [5]. The definitions of CT semantic features were detailed in Supplementary data. Cohen's Kappa coefficient and intraclass correlation coefficient (ICC) were used to evaluate the interobserver agreement for categorical variables and continuous variables, respectively. Generally, the Kappa coefficient/ICC of 0–0.20 indicates a poor agreement; 0.21–0.40 fair agreement; 0.41–0.60 moderate agreement; 0.61–0.80 good agreement, > 0.80 excellent agreement. The average for the continuous variable was calculated as the final value. For categorical variables, the consensus was reached through discussion if a disagreement occurred.

Radiomics signature development

Image segmentation was performed by two trained radiologists using open-source software of ITK-SNAP (version 3.8.0) as detailed in Supplementary data. Radiomics features were extracted from delineated three-dimensional volume-of-interest of tumors using PyRadiomics software (https://pyradiomics.readthedocs.io/en/latest/index.html). Feature selection and radiomics signature development were detailed in Supplementary data.

DL signature development

We proposed a DL architecture called Swin Transformer to develop a DL signature predictive of LN metastasis. The architecture of the Swin Transformer was depicted as detailed in Fig. 2 and Supplementary data. In data preprocessing, we placed a cubic bounding box on the largest slice of the tumor, ensuring the entire tumor was completely involved within the bounding box. The bounding boxes of images containing the tumors on each CT slice were resampled to 224 × 224 pixels by bilinear interpolation. The bounding boxes of images on three adjacent CT slices were combined into a three-channel image as the input of the DL model to generate the risk probability of LN metastasis. Specifically, to achieve a robust prediction, all three-channel images of each tumor were fed into the DL model, and the average risk probability of LN metastasis was obtained as a DL signature. Transfer learning was used to efficiently develop a Swin Transformer model [29]: the pretraining was performed in 1.28 million natural images from the ImageNet dataset; Afterwards, the developed network was finetuned in 17610 CT images of lung adenocarcinoma in the training cohort. The original code of Swin Transformer is available at https://github.com/microsoft/Swin-Transformer. We implemented the neural network using PyTorch 1.4.1 library in Python 3.7.0 (https://pytorch.org).

Clinical-semantic model and combined model construction

In the training cohort, the significant CS variables in univariate analysis were selected. To avoid multicollinearity, the variables with Spearman correlation coefficients greater than 0.7 were excluded. The remaining CS variables were incorporated

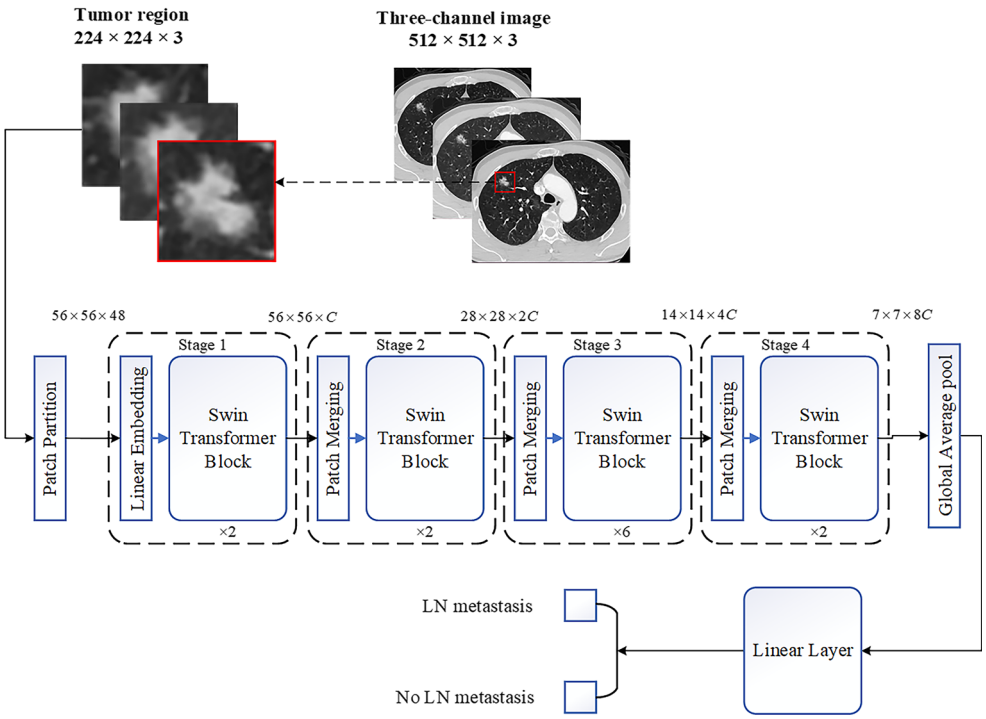

Fig. 2 The detailed architecture of Swin Transformer for prediction of lymph node (LN) metastasis in lung adenocarcinoma

in multivariable logistic regression with forward stepwise selection to determine the independent risk predictors and construct the CS model. Noted that the pathological metrics were recorded but removed from regression analysis due to the inherent study design of preoperative prediction for LN status. To explore the optimum prediction model, we construct three combined models by integrating radiomics signature, DL signature, and both of them with CS model, which were indicated as CS-radiomics model, CS-DL model, and CS-radiomics-DL model.

Statistical analysis

Statistical analysis was conducted using software of MATLAB (MathWorks Inc.) and SPSS (IBM, ver. 26.0). The continuous variables were tested for normality and homogeneity of variance using the Shapiro-Wilk test and Levene test, respectively. The continuous variables were compared using the Student's t-test and ANOVA test, or Mann-Whitney U test and Kruskal-Wallis test, as appropriate. The categorical variables were compared using the chi-square test or Fisher exact test, as appropriate. The correlation between variables was assessed using the Spearman correlation coefficient.

The receiver operating characteristic curve (ROC) was depicted and the area under the curve (AUC) along with sensitivity and specificity were calculated to quantify model performance. The comparisons of AUC were conducted by the DeLong test. The calibration curve and Hosmer-Lemeshow test were used to evaluate the agreement of predicted probabilities with actual observations. The decision curve analysis was depicted to exhibit clinical utility. Two-tailed p value < 0.05 indicated a significant difference.

Results

The clinicopathological characteristics and semantic features among the training cohort ($n = 489$), internal validation cohort ($n = 124$), and independent test cohort ($n = 108$) were similarly distributed as revealed in Table 1. Among the total of 720 patients, 359 (49.9%) were male (median age (interquartile): 60.0 (53, 65)) and 361 (50.1%) were female (median age (interquartile): 59.0 (52.0, 65.0)). Totally, pathologically-confirmed LN metastasis occurred in 199 (27.6%) out of 720 patients. Of them, there were 49 (24.6%), 143 (71.9%), and 7 (3.5%) patients diagnosed with N1, N2, and N3 disease, respectively. The negative LNs were pathologically confirmed to be inflammatory proliferation, tuberculous granuloma, sarcoidosis, or normal nodal pathological structure.

Interobserver agreement assessment of semantic features

The ICCs for tumor total diameter, tumor consolidation diameter and CTR were 0.985 (95% confidence interval [CI]: 0.975, 0.990), 0.989 (95% CI: 0.979, 0.993), and 0.990 (95% CI: 0.988, 0.991), respectively, which were indicative of excellent agreement. The disagreement numbers and percentages between two radiologists occurring for categorial

Table 1 The distribution of clinicopathological characteristics and semantic features across the training cohort, internal validation cohort, and independent test cohort

Variable	Training cohort (n = 489)	Internal validation cohort (n = 123)	Independent test cohort (n = 108)	p value
A. Clinical characteristics				
Age* (year)	60.0 (52.5, 64.0)	59.0 (53.0, 66.0)	58.5 (51.3, 66.0)	0.712
Gender				0.277
Female	248 (50.7%)	66 (53.7%)	47 (43.5%)	
Male	241 (49.3%)	57 (46.3%)	61 (56.5%)	
Smoking history				0.541
Nonsmoker	308 (63.0%)	79 (64.2%)	64 (59.3%)	
Former smoker	65 (13.3%)	21 (17.1%)	19 (17.6%)	
Current smoker	116 (23.7%)	23 (18.7%)	25 (23.1%)	
Pack-year				0.947
≤ 3	321 (65.7%)	80 (65.0%)	67 (62.0%)	
4–40	119 (24.3%)	32 (26.0%)	29 (26.9%)	
> 40	49 (10.0%)	11 (9.0%)	12 (11.1%)	
CEA (ug/L)				0.416
≤ 5	370 (75.7%)	87 (70.7%)	84 (77.8%)	
> 5	119 (24.3%)	36 (29.3%)	24 (22.2%)	
B. Pathological characteristics				
Histological grade				0.102
Low (LPA)	87 (17.8%)	19 (15.5%)	22 (20.4%)	
Intermediate (APA + PPA)	339 (69.3%)	80 (65.0%)	78 (72.2%)	
High (SPA + MPA)	63 (12.9%)	24 (19.5%)	8 (7.4%)	
Ki-67 LI* (%)	10.0 (5.0, 30.0)	18.3 (10.0, 30.0)	10.0 (5.8, 20.0)	0.461
Ki-67 LI				0.101
< 10%	161 (32.9%)	30 (24.4%)	28 (25.9%)	
≥ 10%	328 (67.1%)	93 (75.6%)	80 (74.1%)	
Pathologically-confirmed LN status				0.761
Negative	356 (72.8%)	90 (73.2%)	75 (69.4%)	
Positive	133 (27.2%)	33 (26.8%)	33 (30.6%)	
C. Semantic features				
Location				0.062
Central	102 (20.9%)	15 (12.2%)	17 (15.7%)	
Peripheral	387 (79.1%)	108 (87.8%)	91 (84.3%)	
Affiliated lobe				0.128
Upper lobe	292 (59.7%)	71 (57.7%)	53 (49.1%)	
Middle/lower lobe	197 (40.3%)	52 (42.3%)	55 (50.9%)	
Tumor total diameter* (mm)	24.0 (20.0, 31.0)	25.0 (19.0, 33.0)	25.0 (18.0, 32.0)	0.850
Tumor consolidation diameter* (mm)	22.0 (14.0, 29.0)	21.0 (14.0, 31.0)	23.0 (14.0, 29.8)	0.970
CTR* (%)	100.0 (68.2, 100.0)	100.0 (66.7, 100.0)	100.0 (73.5, 100.0)	0.891
CTR				0.964
0	18 (3.7%)	5 (4.1%)	4 (3.7%)	
1–50%	39 (8.0%)	13 (10.6%)	8 (7.4%)	
51–99%	145 (29.6%)	32 (26.0%)	32 (29.6%)	
100%	287 (58.7%)	73 (59.3%)	64 (59.3%)	
Presence of spiculation	366 (74.8%)	94 (76.4%)	82 (75.9%)	0.923
Presence of lobulation	472 (96.5%)	119 (96.7%)	104 (96.3%)	0.983
Presence of air bronchogram	228 (46.6%)	61 (49.6%)	48 (44.4%)	0.729
Presence of pleural attachment	153 (31.3%)	37 (30.1%)	27 (25.0%)	0.436

Table 1 (continued)

Variable	Training cohort (n = 489)	Internal validation cohort (n = 123)	Independent test cohort (n = 108)	p value
LN short-axis diameter* (mm)	8 (7, 9)	8 (7, 9)	8 (6, 9)	0.438
CT-reported LN status				0.441
Negative	408 (83.4%)	97 (78.9%)	91 (84.3%)	
Positive	81 (16.6%)	26 (21.1%)	17 (15.7%)	

Unless otherwise stated, data were presented as numbers (percentages) and compared using the Chi-square test or Fisher's exact test

* Data were presented as medians (inter-quartiles) and compared using the Kolmogorov-Smirnov test.

CEA carcinoembryonic antigen, *CTR* consolidation-to-tumor ratio, *LPA* lepidic predominant adenocarcinoma, *APA* acinar predominant adenocarcinoma, *PPA* papillary predominant adenocarcinoma, *SPA* solid predominant adenocarcinoma, *MPA* micropapillary predominant adenocarcinoma, *LI* labeling index, *LN* lymph node

variables were shown in Table 2. Cohen's Kappa coefficients for categorical variables also showed good agreement as detailed in Table 2.

The development of radiomics signature and DL signature

Totally, 1210 radiomics features were extracted and selected as detailed in Supplementary data. Finally, an eighteen-feature radiomics signature was generated by a linear combination of the selected features weighted by their respective regression coefficients as detailed in Supplementary data. The DL output of the last layer of the Swin Transformer was obtained as the DL signature.

Clinical-semantic model and combined model construction

In Table 3, patients with CEA > 5 ug/L were prone to suffer from LN metastasis ($p < 0.001$), but no association of age, gender, smoking history, and pack-year with LN metastasis was observed. LN metastasis was more common in patients with intermediate- and high-grade lung adenocarcinoma ($p < 0.001$); The Ki-67 LI in patients with LN metastasis was higher than that in patients without LN metastasis ($p < 0.001$). LN metastasis was more frequently found in tumors with a larger total diameter and consolidation diameter, higher CTR, spiculation, pleural attachment, and CT-reported LN metastasis, and less common in tumors with air bronchogram (all $p < 0.001$).

CEA, tumor total diameter, tumor consolidation diameter, CTR, spiculation, air bronchogram, pleural attachment, and CT-reported LN metastasis were the candidates to construct the CS model. Tumor consolidation diameter was excluded owing to a strong correlation with tumor total diameter as revealed in Fig. 3 ($r = 0.81$, $p < 0.001$). Finally, CEA > 5 ug/L (odds ratio [OR]: 2.758; 95% CI: 1.670, 4.555; $p < 0.001$), CTR (OR: 1.062; 95% CI: 1.038, 1.086; $p < 0.001$), air bronchogram (OR: 0.582; 95% CI: 0.355, 0.951; $p = 0.031$), pleural attachment (OR: 1.748; 95% CI:

Table 2 The interobserver agreement of CT semantic features for lung adenocarcinoma

CT semantic feature	Disagreement	Kappa value/ICC	95% CI
Location‡	31 (4.3%)	0.857	0.808, 0.906
Affiliated lobe‡	4 (0.6%)	0.989	0.977, 1.000
Tumor total diameter§	NA	0.985	0.975, 0.990
Tumor consolidation diameter§	NA	0.989	0.979, 0.993
CTR§	NA	0.990	0.988, 0.991
Spiculation‡	41 (5.7%)	0.847	0.802, 0.892
Lobulation‡	10 (1.4%)	0.826	0.720, 0.932
Air bronchogram‡	49 (6.8%)	0.863	0.826, 0.900
Pleural attachment‡	16 (2.2%)	0.947	0.922, 0.972
CT-reported LN metastasis‡	13 (1.8%)	0.938	0.901, 0.975

§ ICC was calculated for the continuous variables

‡ Cohen's kappa coefficient was calculated for the categorical variables

Disagreement was presented as numbers (percentages)

ICC intraclass correlation coefficient, *CTR* consolidation-to-tumor ratio, *CI* interval confidence, *NA* not applicable

Table 3 Univariate analysis of clinicopathological characteristics, semantic features, radiomics signature, and deep learning signature in training cohort

Variable	LN metastasis (n = 133)	No LN metastasis (n = 356)	p value
A. Clinical characteristics			
Age* (year)	60.0 (53.0, 64.0)	59.0 (52.0, 65.0)	0.531
Gender			0.618
Female	65 (48.9%)	183 (51.4%)	
Male	68 (51.1%)	173 (48.6%)	
Smoking history			0.418
Nonsmoker	80 (60.2%)	228 (64.0%)	
Former smoker	16 (12.0%)	49 (13.8%)	
Current smoker	37 (27.8%)	79 (22.2%)	
Pack-year			0.885
≤ 3	85 (63.9%)	236 (66.3%)	
4–40	34 (25.6%)	85 (23.9%)	
> 40	14 (10.5%)	35(9.8%)	
CEA (ug/L)			< 0.001
≤ 5	75 (56.4%)	295 (82.9%)	
> 5	58 (43.6%)	61 (17.1%)	
B. Pathological characteristics			
Histological grade			< 0.001
Low	3 (2.3%)	84 (23.6%)	
Intermediate	106 (79.7%)	233 (65.4%)	
High	24 (18.0%)	39 (11.0%)	
Ki-67 LI* (%)	20.0 (10.0, 30.0)	10.0 (5.0, 20.0)	< 0.001
Ki-67 LI			< 0.001
< 10%	12 (9.0%)	149 (41.9%)	
≥ 10%	121 (91.0%)	207 (58.1%)	
C. Semantic features			
Location			0.069
Central	35 (26.3%)	67 (18.8%)	
Peripheral	98 (73.7%)	289 (81.2%)	
Affiliated lobe			0.458
Upper lobe	83 (62.4%)	209 (58.7%)	
Middle/lower lobe	50 (37.6%)	147 (41.3%)	
Tumor total diameter* (mm)	28.0 (22.0, 33.0)	23.0 (19.0, 30.0)	< 0.001
Tumor consolidation diameter* (mm)	27.0 (21.5, 32.0)	19.0 (12.0, 26.0)	< 0.001
CTR* (%)	100.0 (100.0, 100.0)	87.2 (57.2, 100.0)	< 0.001
CTR			< 0.001
0	0	18 (5.0%)	
1–50%	0	39 (11.0%)	
51–99%	15 (11.3%)	130 (36.5%)	
100%	118 (88.7%)	169 (47.5%)	
Presence of spiculation	117 (88.0%)	249 (69.9%)	< 0.001
Presence of lobulation	129 (97.0%)	343 (96.3%)	0.729
Presence of air bronchogram	42 (31.6%)	186 (52.2%)	< 0.001
Presence of pleural attachment	60 (45.1%)	93 (26.1%)	< 0.001
LN short-axis diameter* (mm)	9 (8, 13.5)	8 (7, 9)	< 0.001
CT-reported LN status			< 0.001
Negative	88 (66.2%)	320 (89.9%)	
Positive	45 (33.8%)	36 (10.1%)	

Table 3 (continued)

Variable	LN metastasis (n = 133)	No LN metastasis (n = 356)	p value
Radiomic signature	1.430 (0.421, 2.856)	−1.486 (−2.670, −0.287)	< 0.001
Deep learning signature	0.602 (0.544, 0.677)	0.280 (0.216, 0.356)	< 0.001

Unless otherwise stated, data were presented as numbers (percentages) and compared using the chi-square test or Fisher's exact test

* Data were presented as medians (inter-quartiles) and compared using the Mann-Whitney U test

CEA carcinoembryonic antigen, *LI* labeling index, *CTR* consolidation-to-tumor ratio, *LN* lymph node

1.074, 2.844; p = 0.025), and CT-reported LN status (OR: 4.511; 95% CI: 2.495, 8.155; p < 0.001) as the independent risk predictors were incorporated to construct CS model. Accordingly, the combined CS-Radiomics model, CS-DL model, and CS-radiomics-DL model were constructed as revealed in Table 4.

Model performance evaluation

There were 68 patients occurring the LN metastasis out of all 124 patients with CT-reported LN metastasis. The other patients without LN metastasis were pathologically diagnosed to be inflammatory proliferative diseases, tuberculous granuloma, sarcoidosis, or normal pathological structure. In Table 5, CT-reported LN status alone performed far inferior to CS model in all three cohorts (AUC: 0.619 vs. 0.823 for training cohort, p < 0.001; 0.604 vs. 0.781 for internal validation cohort, p = 0.026; 0.627 vs. 0.853 for independent test cohort, p < 0.001). The sensitivity of CT-reported LN status ranged from 0.303 to 0.394, while the specificity ranged from 0.844 to 0.907 in diagnosing LN metastasis across three cohorts.

The AUC for CS model was 0.823 (95% CI: 0.785, 0.861) in training cohort, 0.781 (95% CI: 0.693, 0.869) in internal validation cohort, and 0.853 (95% CI: 0.780, 0.926) in independent test cohort. The AUC for radiomics signature was 0.884 (95% CI: 0.853, 0.915) in training cohort, 0.863 (95% CI: 0.787, 0.939) in internal validation cohort, and 0.886 (95% CI: 0.826, 0.946) in independent test cohort.

Encouragingly, DL signature achieved significantly higher AUC than CS model and radiomics signature in training cohort (0.961 vs. 0.823, p < 0.001; 0.961 vs. 0.884, p < 0.001),

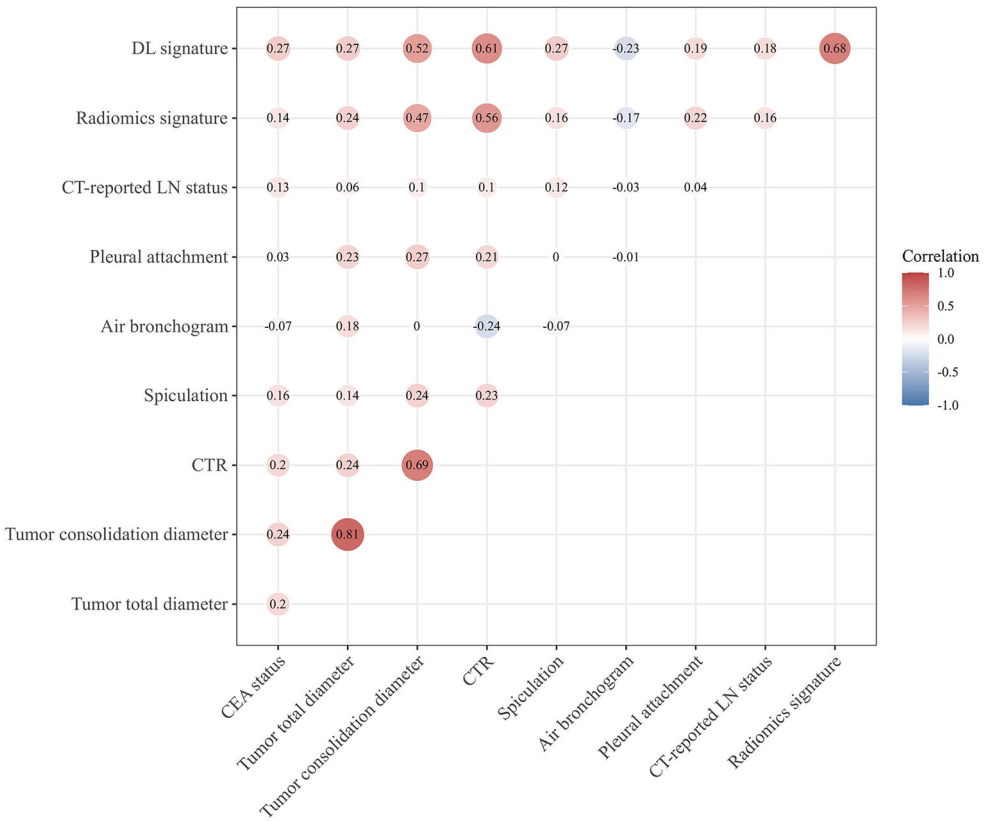

Fig. 3 The pairwise correlation evaluation of clinical-semantic (CS) candidate variables, radiomics signature and deep learning (DL) signature using Spearman correlation coefficient

Table 4 Multivariable logistic regression analyses of the CS model and combined models for predicting lymph node metastasis

Variable	CS model		CS-radiomics model		CS-DL model		CS-radiomics-DL model	
	OR (95% CI)	*p* value	OR (95% CI)	*p* value	OR (95% CI)	*p* value	OR (95% CI)	*p* value
CEA > 5 ug/L	2.758 (1.670, 4.555)	< 0.001	3.876 (2.121, 7.081)	< 0.001	2.690 (1.225, 5.911)	0.014	3.275 (1.402, 7.653)	0.006
CTR	1.062 (1.038, 1.086)	< 0.001	1.036 (1.009, 1.063)	0.007	NA	0.195	NA	0.578
Air bronchogram	0.582 (0.355, 0.951)	0.031	NA	0.054	NA	0.211	NA	0.180
Pleural attachment	1.748 (1.074, 2.844)	0.025	NA	0.563	NA	0.361	NA	0.961
CT-reported LN metastasis	4.511 (2.495, 8.155)	< 0.001	4.153 (2.096, 8.226)	< 0.001	4.202 (1.575, 11.213)	0.004	3.304 (1.166, 9.363)	0.025
Radiomics signature	NA	NA	2.176 (1.809, 2.616)	< 0.001	NA	NA	1.607 (1.280, 2.018)	< 0.001
DL signature × 10	NA	NA	NA	NA	6.436 (4.499, 9.207)	< 0.001	5.208 (3.588, 7.558)	< 0.001

Noted that the results were based on the training cohort. *CEA* carcinoembryonic antigen, *CTR* consolidation-to-tumor ratio, *DL* deep learning, *CS* clinical-semantic, *OR* odds ratio, *CI* confidence interval, *NA* not applicable

internal validation cohort (0.948 vs. 0.781, $p < 0.001$; 0.948 vs. 0.863, $p = 0.019$), and independent test cohort (0.960 vs. 0.853, $p = 0.002$; 0.960 vs. 0.886, $p = 0.029$), respectively (Fig. 4A–C). The sensitivity and specificity of DL signature in predicting LN metastasis ranged from 0.758 to 0.910 and 0.907 to 0.987 across all three cohorts, respectively.

The Hosmer-Lemeshow tests ($p = 0.267$ for the training cohort, $p = 0.790$ for the internal validation cohort, and $p = 0.754$ for the independent test cohort) and the calibration curves revealed DL signature predicted probabilities had a good agreement with the actual observed probabilities in all three cohorts (Fig. 4E–G). From decision curve analyses, the

Table 5 The model performances in the training cohort, internal validation cohort and independent test cohort

Model	AUC (95% CI)	Sensitivity (95% CI)	Specificity (95% CI)
Training cohort			
CT-reported LN status	0.619 (0.559, 0.678)	0.338 (0.263, 0.422)	0.899 (0.863, 0.926)
CS model	0.823 (0.785, 0.861)	0.910 (0.848, 0.953)	0.573 (0.520, 0.625)
Radiomics signature	0.884 (0.853, 0.915)	0.880 (0.812, 0.930)	0.758 (0.711, 0.802)
DL signature	0.961 (0.942, 0.979)	0.910 (0.848, 0.953)	0.907 (0.872, 0.935)
CS-radiomics model	0.914 (0.888, 0.939)	0.910 (0.848, 0.953)	0.801 (0.755, 0.841)
CS-DL model	0.965 (0.948, 0.983)	0.865 (0.795, 0.918)	0.961 (0.935, 0.978)
CS-radiomics-DL model	0.974 (0.959, 0.988)	0.910 (0.848, 0.953)	0.938 (0.908, 0.961)
Internal validation cohort			
CT-reported LN status	0.604 (0.486, 0.722)	0.394 (0.222, 0.534)	0.844 (0.756, 0.905)
CS model	0.781 (0.693, 0.869)	0.697 (0.513, 0.844)	0.767 (0.666, 0.849)
Radiomics signature	0.863 (0.787, 0.939)	0.818 (0.645, 0.930)	0.833 (0.740, 0.904)
DL signature	0.948 (0.910, 0.987)	0.758 (0.577, 0.889)	0.967 (0.906, 0.993)
CS-radiomics model	0.882 (0.811, 0.954)	0.848 (0.681, 0.949)	0.844 (0.753, 0.912)
CS-DL model	0.958 (0.921, 0.995)	0.848 (0.681, 0.949)	0.978 (0.922, 0.997)
CS-radiomics-DL model	0.958 (0.920, 0.996)	0.848 (0.681, 0.949)	0.989 (0.940, 1.000)
Independent test cohort			
CT-reported LN status	0.627 (0.505, 0.748)	0.303 (0.197, 0.504)	0.907 (0.836, 0.963)
CS model	0.853 (0.780, 0.926)	0.697 (0.513, 0.844)	0.827 (0.722, 0.904)
Radiomics signature	0.886 (0.826, 0.946)	0.970 (0.842, 0.999)	0.693 (0.576, 0.795)
DL signature	0.960 (0.922, 0.997)	0.818 (0.645, 0.930)	0.987 (0.928, 1.000)
CS-radiomics model	0.936 (0.893, 0.979)	0.879 (0.718, 0.966)	0.853 (0.753, 0.924)
CS-DL model	0.958 (0.918, 0.997)	0.848 (0.681, 0.949)	0.973 (0.907, 0.997)
CS-radiomics-DL model	0.969 (0.938, 1.000)	0.879 (0.718, 0.966)	0.947 (0.869, 0.985)

CS clinical-semantic, *DL* deep learning, *AUC* area under the receiver operating characteristic curve, *CI* confidence interval

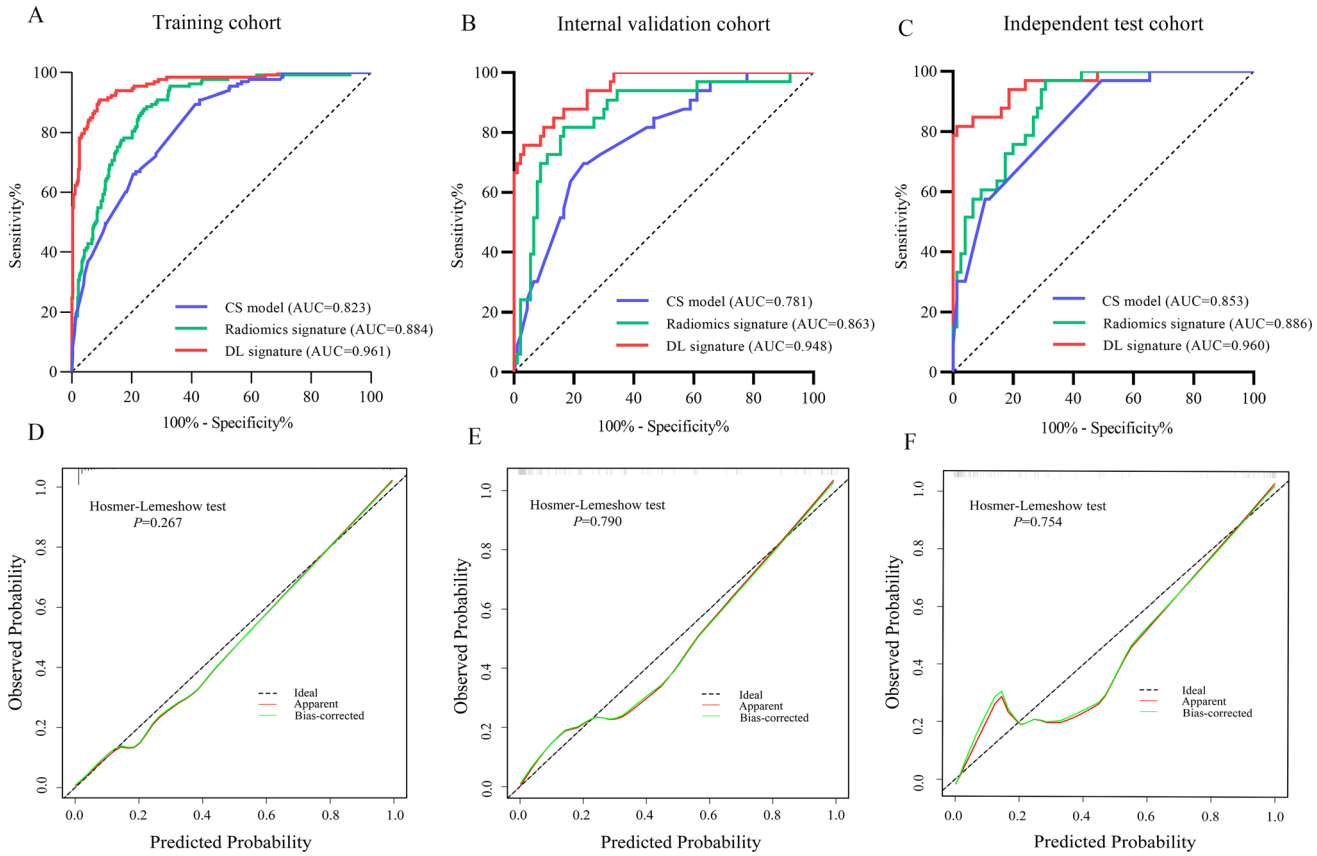

Fig. 4 The performance evaluation of DL signature in predicting LN metastasis. (**A–C**) The receiver operating characteristic curves of CS model, radiomics signature and DL signature in training cohort (**A**), internal validation cohort (**B**), and independent test cohort (**C**). Number in parenthesis is the area under receiver operating characteristic curve. (**D–F**) The calibration curves depicted the agreements between DL signature predicted probabilities and actual observed probabilities of LN metastasis in training cohort (**D**), internal validation cohort (**E**), and independent test cohort (**F**)

DL signature could confer a higher net benefit in predicting LN metastasis than the CS model and radiomics signature across the threshold probability range of 0.2–1.0 (Fig. 5).

In the training cohort, the combined CS-radiomics model, CS-DL model, and CS-radiomics-DL model achieved an AUC of 0.914, 0.965, and 0.974, respectively. In the internal validation cohort, the combined CS-radiomics model, CS-DL model, and CS-radiomics-DL model achieved an AUC of 0.882, 0.958, and 0.958, respectively. In the independent test cohort, the AUCs for the aforementioned models were 0.936, 0.958, and 0.969, respectively. Reasonably, the inclusion of radiomics signature, DL signature, or both of them showed an incremental value with respect to the CS model in all three cohorts (all $p < 0.05$). In training cohort, CS-Radiomics-DL model performed slightly superior to DL signature (0.974 vs. 0.961, $p = 0.005$), but AUCs for CS-DL model and DL signature were comparable (0.965 vs. 0.961, $p = 0.107$). Furthermore, in internal validation cohort and independent test cohort, no significant difference was observed between the DL signature and three combined models (all $p > 0.05$); in other words, the incorporation of CS risk predictors and radiomics signature did not reveal a substantial improvement in discriminative performance over DL signature.

Discussion

This study developed a DL signature predictive of invasive mediastinal metastasis based on a novel Swin-Transformer architecture, yielding an AUC of 0.961 (95% CI: 0.942, 0.979), 0.948 (95% CI: 0.910, 0.987), and 0.960 (95% CI: 0.922, 0.997) in the training cohort, internal validation cohort, and independent test cohort, respectively. The proposed DL signature exhibited superior predictive efficacy to the traditional CS model and radiomics signature. Furthermore, the DL signature acquired a higher net benefit than both the CS model and radiomics signature.

Currently, there is limited literature on adopting the DL technique in presurgical prediction for LN staging in lung cancer. Ran et al used VGG-6 to generate a DL signature predictive of LN metastasis, which yielded an AUC of 0.812 in the external validation set [24]; Zhao et al presented a DL

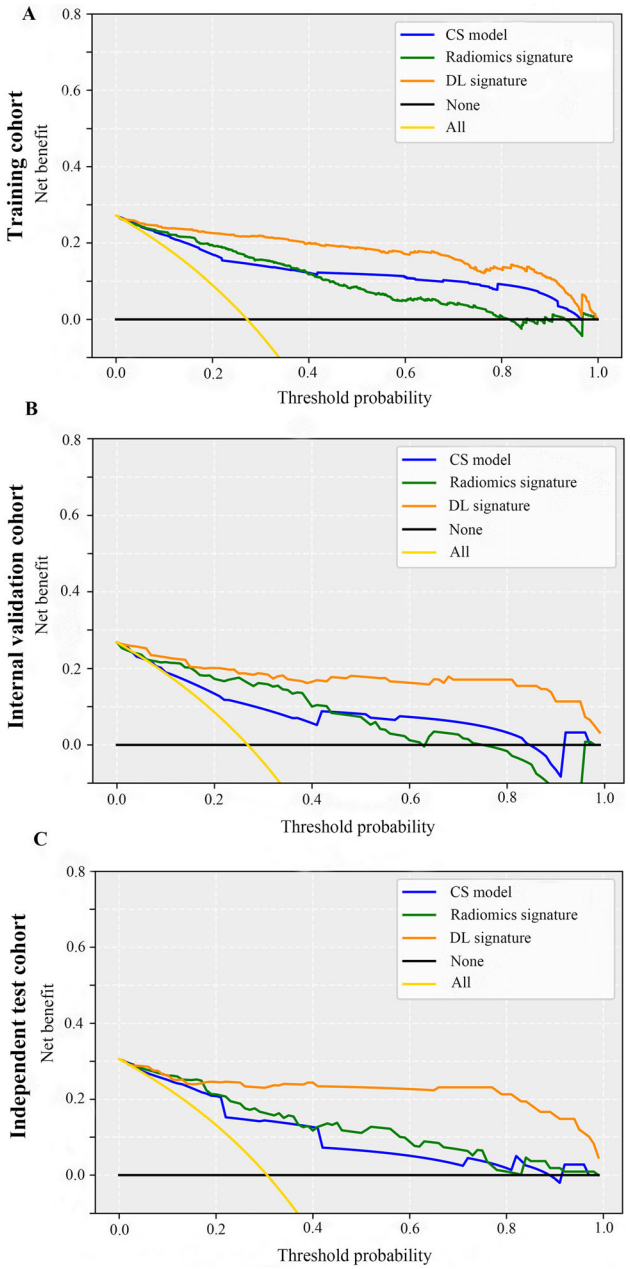

Fig. 5 Decision curve analyses of CS model, radiomics signature and DL signature in training cohort (**A**), internal validation cohort (**B**), and independent test cohort (**C**). DL signature conferred a higher net benefit in predicting LN metastasis than CS model and radiomics signature across threshold probability range of 0.2–1.0

framework named DenseNet algorithm for risk estimation of occult LN metastasis, resulting in an AUC of 0.880 [23]. Our developed DL signature achieved an AUC ranging from 0.948 to 0.961 across all cohorts, far exceeding the previous DL results. This remarkable capability may attribute to the state-of-the-art Swin Transformer architecture serving as the backbone of our DL model, which was exploited by Liu and colleagues from Microsoft Research Asia in 2021 [30]. Swin Transformer has two key strengths: hierarchical feature representation and multi-head self-attention based on shifted windows. This hierarchical architecture limits self-attention computation to non-overlapping shifted windows and allows cross-window connections, which can be flexibly applied in modeling at various scales. The Swin Transformer has been proved highly efficient in image classification, dense detection, and semantic segmentation [30].

For comparison with the DL signature, a radiomics signature was generated by a linear polynomial of eighteen selected features. The AUC for radiomics signature ranged from 0.863 to 0.886 in this study, far inferior to that for DL signature in the corresponding cohort. Radiomics technique relies strongly on delicate delineation generally performed by trained radiologists, which overburdens clinical workload. Radiomics processing involves several sequential steps including tumor segmentation, feature extraction, feature selection, and model establishment, and the overall modeling performance depends on the processing quality of each step. These qualities consequently contribute to a disadvantage of confined generalization capability and limited ability to leverage high-throughput features in radiomics. DL is an end-to-end architecture, where models are adjusted and finally converged by reversely transmitting the errors between predicted results and real observations in each layer. Aside from that, the DL technique is characterized by automatic representative data acquisition, free from clinical index collection, semantic feature interpretation, and manual annotation, and therefore is readily accepted in clinical workflow [31–33].

To construct a CS model predictive of LN metastasis, we modestly considered the potential clinical variables and CT semantic features. As a cell adhesion-associated glycoprotein, CEA is widely considered an indicator of tumor invasiveness and plays an important role in prognosis evaluation and treatment monitoring for lung cancer [34, 35]. Multivariable logistic regression analyses revealed that elevated serum CEA (> 5 ug/L) was independently associated with LN metastasis in both the CS model and combined models. Consistent with our findings, Wang et al [12] and Gu et al [36] also demonstrated that CEA was the independent risk predictor for LN metastasis when incorporating CS features and radiomics signature. CTR is a quantitative manifestation of consolidation proportion within tumors [37]. Prior studies confirmed that CTR was of great value in predicting LN metastasis for lung adenocarcinoma [6, 38]. In the CS model, CTR was an independent risk predictor for LN metastasis, with a 1.82-fold increased risk of LN metastasis for every 10% increase in CTR. However, CTR became insignificant when integrating DL signature with the CS model. The strong correlation between DL signature and CTR ($r = 0.611$, $p < 0.001$) might account for this. Beyond that, air bronchogram and pleural attachment were closely associated with LN metastasis, which were previously reported to be radiological markers reflecting tumor aggressiveness [39, 40]. CT-reported LN status is a conventional assessment metric for clinical mediastinal

staging, depending on macroscopic measurement for LN short-axis diameter [41]. Expectedly, CT-reported LN status was weighted heavily in logistic regression equations, but this subjective method revealed poor sensitivity and unsatisfactory AUC in this study. A previous study demonstrated more than 20% of lymph nodes with a short-axis diameter < 1 cm were proved to be tumor involved [42]. CT alone for mediastinal staging is insufficient to meet the requirements of clinical application [12, 43]. Furthermore, the AUCs for the CS model were 0.781–0.853, much poorer than those for the DL signature. Aokage et al constructed a prediction model including tumor diameter, CTR, and solid component density, and created a formula for calculating the probability of LN metastasis in lung adenocarcinoma [6]; He et al found that CEA, lung adenocarcinoma, absence of vascular convergence and pleural attachment were independently predictive of LN metastasis in NSCLC. But these models relied on subjective evaluation by experienced radiologists and achieved the AUCs (0.796–0797) far inferior to our DL signature.

We attempted to exploit the optimum prediction model by a combination of CS risk predictors and radiomics signature with DL signature. It was originally assumed that the inclusion of CT-reported LN status might partially compensate for the deficiency of DL signature in obtaining representative information solely from the tumor region and thus yield a performance improvement over DL signature alone. Nevertheless, the results demonstrated that neither CT-reported LN status nor other CS risk predictors nor radiomics signature conferred an incremental value with regards to DL signature. This finding further lent support to the predominant potency of our proposed DL signature in the prediction of LN metastasis in lung adenocarcinoma.

There were several limitations to this study. First, an important weakness of DL was that small perturbations from data quality and provenance might result in output mistakes. DL signature might be affected by acquisition parameters across multi-vender and multi-institution CT scanners. The present study data were merely from a single center, and larger sample-size, multi-institution datasets should be warranted to affirm the reproducibility and generalization of the developed DL and radiomics signatures. Second, this study only included patients with lung adenocarcinoma. The value of DL signature in predicting other pathological subtypes of lung cancer should be further elucidated. Besides, only a few of our retrospectively enrolled cases received PET-CT scanning, and we temporarily failed to compare the performance of DL signature with PET-CT due to the excessive missing records in PET-CT. However, the discussion on the predictive performance of PET-CT, as well as the incremental predictive value of DL signature with respect to PET-CT should be supplemented in future research. Last, the lack of interpretation of DL results is a major obstacle to the practical application of DL models in clinical practice. The potential biological mechanism underlying the black box of DL signature requires further in-depth investigation. The common method to improve the explanation about DL prediction is to generate a visual feature heatmap using Grad-CAM and explore the clinical diagnosis and decision-making significance of the attention regions. Besides, uncovering some potential biological implications such as relating DL signature with expression of specific genes or proteins predictive of clinical endpoints could further provide the biological interpretability of DL.

In conclusion, we proposed a novel Swin Transformer to develop a DL signature for the prediction of LN metastasis in lung adenocarcinoma, and the predictive efficiency of the DL signature surpassed that of the traditional CS model and radiomics signature. DL signature might serve as an effective tool for non-invasive mediastinal LN staging and in facilitating the formulation of individualized therapeutic strategy.

Supplementary Information The online version contains supplementary material available at https://doi.org/10.1007/s00330-022-09153-z.

Funding This study has received funding from the National Natural Science Foundation of China (NO.81873889).

Declarations

Guarantor The scientific guarantor of this publication is Liming Xia.

Conflict of interest The authors of this manuscript declare no relationships with any companies whose products or services may be related to the subject matter of the article.

Statistics and biometry No complex statistical methods were necessary for this paper.

Informed consent Written informed consent was waived by the Institutional Review Board.

Ethical approval Institutional Review Board approval was obtained.

Study subjects or cohorts overlap Some study subjects or cohorts have been previously reported in a prior study, where 182 patients with early-stage lung adenocarcinoma were previously reported on the relationship between CT morphological features and Ki-67 (PMID: 34164176). The present study has a much larger sample size and focuses on predicting lymph node metastasis in lung adenocarcinoma.

Methodology
- retrospective
- diagnostic study
- performed at one institution

References

1. Siegel RL, Miller KD, Jemal A (2020) Cancer statistics, 2020. CA Cancer J Clin 70(1):7–30
2. Chiang XH, Hsu HH, Hsieh MS et al (2020) Propensity-matched analysis comparing survival after sublobar resection and lobectomy for cT1N0 lung adenocarcinoma. Ann Surg Oncol 27(3):703–715
3. Altorki NK, Wang X, Wigle D et al (2018) Perioperative mortality and morbidity after sublobar versus lobar resection for early-stage non-small-cell lung cancer: post-hoc analysis of an international, randomised, phase 3 trial (CALGB/Alliance 140503). Lancet Respir Med 6(12):915–924
4. Zhang B, Liu R, Ren D et al (2021) Comparison of lobectomy and sublobar resection for stage IA elderly NSCLC patients (≥70 Years): a population-based propensity score matching's study. Front Oncol 11:610638
5. Suzuki K, Koike T, Asakawa T et al (2011) A prospective radiological study of thin-section computed tomography to predict pathological noninvasiveness in peripheral clinical IA lung cancer (Japan Clinical Oncology Group 0201). J Thorac Oncol 6(4):751–756
6. Aokage K, Suzuki K, Wakabayashi M et al (2021) Predicting pathological lymph node status in clinical stage IA peripheral lung adenocarcinoma. Eur J Cardiothorac Surg 60(1):64–71
7. Choi H, Kim H, Park CM, Kim YT, Goo JM (2021) Central tumor location at chest CT is an adverse prognostic factor for disease-free survival of node-negative early-stage lung adenocarcinomas. Radiology 299(2):438–447
8. Prabhakar B, Shende P, Augustine S (2018) Current trends and emerging diagnostic techniques for lung cancer. Biomed Pharmacother 106:1586–1599
9. Kandathil A, Kay FU, Butt YM, Wachsmann JW, Subramaniam RM (2018) Role of FDG PET/CT in the eighth edition of TNM staging of non-small cell lung cancer. Radiographics 38(7):2134–2149
10. Pak K, Park S, Cheon GJ et al (2015) Update on nodal staging in non-small cell lung cancer with integrated positron emission tomography/computed tomography: a meta-analysis. Ann Nucl Med 29(5):409–419
11. Liu Y, Kim J, Balagurunathan Y et al (2018) Prediction of pathological nodal involvement by CT-based Radiomic features of the primary tumor in patients with clinically node-negative peripheral lung adenocarcinomas. Med Phys 45(6):2518–2526
12. Wang X, Zhao X, Li Q et al (2019) Can peritumoral radiomics increase the efficiency of the prediction for lymph node metastasis in clinical stage T1 lung adenocarcinoma on CT? Eur Radiol 29(11):6049–6058
13. Cong M, Feng H, Ren J-L et al (2020) Development of a predictive radiomics model for lymph node metastases in pre-surgical CT-based stage IA non-small cell lung cancer. Lung Cancer 139:73–79
14. He L, Huang Y, Yan L et al (2019) Radiomics-based predictive risk score: a scoring system for preoperatively predicting risk of lymph node metastasis in patients with resectable non-small cell lung cancer. Chin J Cancer Res 31(4):641–652
15. Peng X, Yang S, Zhou L et al (2021) Repeatability and reproducibility of computed tomography radiomics for pulmonary nodules: a multicenter phantom study. Invest Radiol 57(4):242–253
16. Han Y, Ma Y, Wu Z et al (2021) Histologic subtype classification of non-small cell lung cancer using PET/CT images. Eur J Nucl Med Mol Imaging 48(2):350–360
17. Chaunzwa TL, Hosny A, Xu Y et al (2021) Deep learning classification of lung cancer histology using CT images. Sci Rep 11(1):5471
18. Avanzo M, Gagliardi V, Stancanello J et al (2021) Combining computed tomography and biologically effective dose in radiomics and deep learning improves prediction of tumor response to robotic lung stereotactic body radiation therapy. Med Phys 48(10):6257–6269
19. Tian P, He B, Mu W et al (2021) Assessing PD-L1 expression in non-small cell lung cancer and predicting responses to immune checkpoint inhibitors using deep learning on computed tomography images. Theranostics 11(5):2098–2107
20. Hou R, Li X, Xiong J et al (2021) Predicting tyrosine kinase inhibitor treatment response in stage IV lung adenocarcinoma patients with EGFR mutation using model-based deep transfer learning. Front Oncol 11:679764
21. Zhong Y, She Y, Deng J et al (2022) Deep learning for prediction of N2 Metastasis and survival for clinical stage I non-small cell lung cancer. Radiology 302(1):200–211
22. Kim H, Goo JM, Lee KH, Kim YT, Park CM (2020) Preoperative CT-based deep learning model for predicting disease-free survival in patients with lung adenocarcinomas. Radiology 296(1):216–224
23. Zhao X, Wang X, Xia W et al (2020) A cross-modal 3D deep learning for accurate lymph node metastasis prediction in clinical stage T1 lung adenocarcinoma. Lung Cancer 145:10–17
24. Ran J, Cao R, Cai J et al (2021) Development and validation of a nomogram for preoperative prediction of lymph node metastasis in lung adenocarcinoma based on radiomics signature and deep learning signature. Front Oncol 11:585942
25. Wang Y-W, Chen C-J, Huang H-C et al (2021) Dual energy CT image prediction on primary tumor of lung cancer for nodal metastasis using deep learning. Comput Med Imaging Graph 91:101935
26. Yan R, Fan X, Xiao Z et al (2022) Inhibition of DCLK1 sensitizes resistant lung adenocarcinomas to EGFR-TKI through suppression of Wnt/β-Catenin activity and cancer stemness. Cancer Lett 531:83–97
27. Yasukawa M, Ohbayashi C, Kawaguchi T et al (2019) Analysis of histological grade in resected lung-invasive adenocarcinoma. Anticancer Res 39(3):1491–1500
28. Yoshizawa A, Sumiyoshi S, Sonobe M et al (2013) Validation of the IASLC/ATS/ERS lung adenocarcinoma classification for prognosis and association with EGFR and KRAS gene mutations: analysis of 440 Japanese patients. J Thorac Oncol 8(1):52–61
29. Agarwal D, Marques G, de la Torre-Díez I et al (2021) Transfer learning for alzheimer's disease through neuroimaging biomarkers: a systematic review. Sensors (Basel) 21(21):7259
30. LIU Z, LIN Y, CAO Y, et al (2021) Swin transformer: hierarchical vision transformer using shifted windows. arXiv Prepr. 2021, arXiv:2103.14030.
31. Le Berre A, Kamagata K, Otsuka Y et al (2019) Convolutional neural network-based segmentation can help in assessing the substantia nigra in neuromelanin MRI. Neuroradiology 61(12):1387–1395
32. Hagiwara A, Fujita S, Ohno Y, Aoki S (2020) Variability and standardization of quantitative imaging: monoparametric to multiparametric quantification, radiomics, and artificial intelligence. Invest Radiol 55(9):601–616
33. Hosny A, Parmar C, Quackenbush J, Schwartz LH, Aerts H (2018) Artificial intelligence in radiology. Nat Rev Cancer 18(8):500–510
34. Dal Bello MG, Filiberti RA, Alama A et al (2019) The role of CEA, CYFRA21-1 and NSE in monitoring tumor response to Nivolumab in advanced non-small cell lung cancer (NSCLC) patients. J Transl Med 17(1):74
35. Jiao Z, Cao S, Li J et al (2021) Clinical associations of preoperative and postoperative serum CEA and lung cancer outcome. Front Mol Biosci 8:686313
36. Gu Y, She Y, Xie D et al (2018) A texture analysis-based prediction model for lymph node metastasis in stage IA lung adenocarcinoma. Ann Thorac Surg 106(1):214–220
37. Kim H, Goo JM, Kim YT, Park CM (2019) Consolidation-to-tumor ratio and tumor disappearance ratio are not independent prognostic factors for the patients with resected lung adenocarcinomas. Lung Cancer 137:123–128

38. Chen Y-C, Lin Y-H, Chien H-C et al (2021) Preoperative consolidation-to-tumor ratio is effective in the prediction of lymph node metastasis in patients with pulmonary ground-glass component nodules. Thoracic Cancer 12(8):1203–1209
39. Zhang Y, Zhao F, Wu M et al (2021) Association of postoperative recurrence with radiological and clinicopathological features in patients with stage IA-IIA lung adenocarcinoma. Eur J Radiol 141: 109802
40. Kim HJ, Cho JY, Lee YJ et al (2019) Clinical significance of pleural attachment and indentation of subsolid nodule lung cancer. Cancer Res Treat 51(4):1540–1548
41. Silvestri GA, Gonzalez AV, Jantz MA et al (2013) Methods for staging non-small cell lung cancer: diagnosis and management of lung cancer, 3rd ed: American College of Chest Physicians evidence-based clinical practice guidelines. Chest 143(5 Suppl): e211S–e250S
42. Leiro-Fernández V, Fernández-Villar A (2021) Mediastinal staging for non-small cell lung cancer. Transl Lung Cancer Res 10(1):496–505
43. Walker CM, Chung JH, Abbott GF et al (2012) Mediastinal lymph node staging: from noninvasive to surgical. AJR Am J Roentgenol 199(1):W54–W64